

RSC Advances

Cytochrome c Assembly on Fullerene Nanohybrid Metal Oxide Ultrathin Films

Journal:	RSC Advances
Manuscript ID	RA-ART-10-2015-021928.R2
Article Type:	Paper
Date Submitted by the Author:	01-Feb-2016
Complete List of Authors:	Lee, Chang; Korea Research Institute of Bioscience and Biotechnology; University of Science & Technology (UST), Nanobiotechnology (Major) Yang, Do-Hyeon; Chungbuk National University, Chemistry; PNS Technologies, Inc. Shin, Min; KAIST, Chemical and Biomolecular Engineering Choi, Sung Mook; PNS Technologies, Inc. Shin, Jae; Chungbuk National University, Chemistry
Subject area & keyword:	Electronic materials < Materials

SCHOLARONE™ Manuscripts

Cytochrome c Assembly on Fullerene Nanohybrid Metal Oxide Ultrathin Films

Do-Hyeon Yang^{a, b}, Min Jae Shin^c, Sung Mook Choi^b, Chang-Soo Lee ^{d,e,*}, and Jae Sup Shin^{a,**}

aDepartment of Chemistry, Chungbuk National University, 48 Gaeshin-dong, Cheongju, Chungbuk, 361-763, Korea
bR&D Lab., PNS Technologies, Inc., 301 Yeonsung University, 34, Yanghwa-ro 37 beon-gil, Manan-gu, Anyang-si, Gyeonggi-do, 439-730, Korea
cDepartment of Chemistry and Biomolecular Engineering, Korea Advanced Institute of Science and Technology (KAIST), Daejeon 305-806, Korea
dBionanotechnology Research Center, Korea Research Institute of Bioscience and Biotechnology (KRIBB), 125 Gwahak-ro, Yuseong-gu, Deajeon 305-806, Korea
eNanobiotechnology (Major), University of Science & Technology (UST), 217 Gajeong-ro, Yuseong-gu, Daejeon 305-350, Korea

^{*} Corresponding author. Tel.: +82-42-879-8446; fax: +82-42-879-8594.

^{**} Co-Corresponding author. Tel.: +82-43-261-2288; fax: +82-43-261-2279. E-mail addresses: cslee@kribb.re.kr (C-S. Lee), jsshin@chungbuk.ac.kr (J. S. Shin).

Abstract

The immobilization of Cyt. c (Cytochrome c) on C₆₀ (fullerene) nanohybrid TiO₂ (titanium dioxide) gel films assembled with C₆₀, Ti(O-ⁿBu)₄ and Cyt. c was realized by the surface sol-gel process. Interestingly, C₆₀ was used without any surface modification of the film formation and exhibited good electrochemical performance. Additionally, the surface morphologies of the TiO2 and TiO2/C60 nanocomposite thin films showed remarkable uniformity over a wide area, however, the surface morphology depends on the deposition of Cyt. c, which densely covers the surface with adsorbed Cyt. c molecules. The cyclic voltammetry of the outer-most fullerene films revealed high stability, as well as, a pair of current peaks characteristic of a weak redox system with anodic and cathodic peak potentials at 0.262 V and 0.137 V. The electrochemical properties of thin films can be attributed to the redox system of the C₆₀ layer deposited on the TiO₂ gel layer. A pair of well-defined quasireversible redox peaks generated by Cyt. c are easily achieved because of the efficient assembly on the C₆₀-modified electrode. In this work, we suggest that the efficient introduction of C₆₀ into the TiO₂ gel matrix, evaluating electrochemical characteristics of Cyt. c assembly.

1. Introduction

Nanocarbon materials, such as fullerenes, carbon nanotubes, and graphene, have attracted a substantial amount of attention in a wide variety of fields because of their extraordinary thermal conductivity and electrical, optical, and mechanical properties [1-7]. For the past decade, abundant research on nanocarbon materials has been conducted, including with regards to their use in nanoelectronic devices [8,9], electrical circuits [10-12], biomedical applications [13-15], energy storage [16,17], nanosensors [18,19], reinforcement materials [20,21], and solar cells [22-25]. Since their discovery in 1985 [26], fullerenes have been a significant subject of intensive research regarding both their unique chemical properties, which are not exhibited by any other existing compounds, and practical applications of their highly symmetric structures with diameters of approximately 1.0 nm and abundant π -electron systems [27]. Therefore, previous studies on fullerenes and their derivatives have focused on functions that are affiliated with superconductors [28,29] and magnetic materials [30]. Recent studies have demonstrated their performance as functional materials, including for biological applications, such as DNA-carrying devices [31,32] and pharmaceuticals [33], and as fuel cells [34,35] and solar cells [36-38].

Moreover, fullerenes have the ability to significantly improve electron-transfer reactions and could be used as an electrode material in electrochemical devices [39,40]. In particular, incorporating noble fullerenes into electrodes is a promising pathway for efficient electrical communications in bioelectronics systems. Thus, a number of studies have focused developing efficient methods for fullerene modification and their effective incorporation into electrodes [41-43]. Chai et al. reported a novel approach for highly sensitive glucose detection using fullerene functionalized spherical Pd@Cys-C₆₀ nanoparticles consisting of L-Cysteine and Pd by an in situ spontaneous reduction process. The electrocatalytic activity of a Pd@Cys-C₆₀ nanoparticle-modified electrode facilitated detection with excellent sensitivity and stability and a fast response to glucose [44]. Zhang et al. demonstrated that fullerenes can promote electron transfer between hemeproteins and electrodes. They developed C₆₀-MWCNT films as nanocomposite materials to facilitate the direct electron transfer of hemoglobin (Hb) more effectively than bare MWCNT films. They reported a faster electron transfer on the C₆₀-MWCNT film and confirmed that the electron mediator and protein docking site roles are played by C₆₀. Hb can transfer electrons to and from electrodes relatively easily through C₆₀ in C₆₀-MWCNT nanocomposite films [45]. Recently, Lanzellotto et al. reported a novel electrochemical biosensing platform based on

nanostructured materials using gold nanoparticles and fullerenols. Modifying the electrode enhanced of the electrochemical properties [46]. The functionalization of fullerenes can be achieved through various free-radical or cycloaddition reactions. Thus, chemical reactions involving fullerenes follow essentially original structure changes, and the π -electron systems deviate substantially from the original ones [47].

Recently, we examined a novel TiO_2 /fullerene nanocomposite thin film assembled with C_{60} and $Ti(O^{-n}Bu)_4$, which was fabricated by a surface sol-gel process to prepare ultrathin metal oxide films. The elemental ratio of C/Ti within the TiO_2/C_{60} film was estimated to be 4.7 by X-ray photoelectron spectroscopy (XPS) measurements, indicating that one C_{60} molecule is surrounded by a matrix of 13 Ti atoms. An important feature of this approach is that fullerene nanohybrid ultrathin films could be controlled at nanometer thicknesses and used in pristine C_{60} [48,49].

In the present study, we explored a new approach for immobilizing Cyt. c on the fullerene nanohybrid TiO₂ gel film, which was developed using a nanoassembly approach, to obtain bioelectrochemical systems of Cyt. c. This approach should provide a potential pathway for not only creating novel bioelectrochemical devices but also fabricating the elements of nanostructure materials.

2. Experimental

2.1 Materials

Titanium (IV)-n-butoxide (Ti(O- n Bu)₄) was purchased from Acros Organics (New Jersey, USA). Fullerene (C₆₀) was obtained from Aldrich. Horse heart cytochrome c (Cyt. c) was purchased from Wako Co. (Tokyo, Japan). Phosphate buffer solution (PBS) was obtained from Samchum Pure Chemical Co. (Pyeongtaek, Korea). 10 mM PBS, pH 7.0, was used for the preparation of Cyt. c electrode, and served for recording of cyclic voltammograms. All of these chemicals were guaranteed reagents, and used without further purification. All of the other chemicals that were used as solvents were of analytical-grade purity and obtained from commercial sources. Pure deionized water (18.2 M Ω ·cm) was obtained by reverse osmosis followed by ion exchange and filtration (AquaMaxTM-Ultra, Younglin Instrument, Korea).

2.2 Preparation of nanohybrid ultrathin films

Gold-coated quartz crystal microbalance (QCM, 9 MHz manufactured by USI System, Japan) electrodes, quartz plates, and silicon wafers were used as substrates for the preparation of thin films. Prior to film assembly, a gold-coated QCM electrode was treated with piranha

solution (96 % sulfuric acid/30.0~35.5 % hydrogen peroxide, 3/1, v/v) and then rinsed with pure water, washed with ethanol and dried under flowing nitrogen gas. The electrode was then treated in an ethanol solution of 2-mercaptoethanol (10 mM) for 12 h, washed with ethanol and water, and dried under flowing with nitrogen gas. Thus, the activated electrode contains free hydroxyl groups on the surface. The QCM frequency was measured with a Hewlett-Packard 53131 A counter (255 Hz), where a 1-Hz frequency decrease corresponds to a mass increase of ca. 0.9 ng, according to the Sauerbrey equation [50].

In the present work, nanohybrid ultrathin films were prepared by the surfaces sol-gel process. First, a hydroxylated QCM electrode was immersed in 100-mM $Ti(O^{-n}Bu)_4$ in toluene/ethanol (1/1, v/v) for 5 min at 25 °C and washed twice with ethanol for 1 min to remove the physically adsorbed $Ti(O^{-n}Bu)_4$. After hydrolysis in deionized water for 1 min and drying under flowing with nitrogen gas, the TiO_2 gel-deposited electrode was immersed into 1-mM C_{60} solution in toluene for 20 min at 25 °C; next, we thoroughly removed the physically adsorbed C_{60} with toluene. By repeating the TiO_2 gel deposition procedures, the outermost surface of the TiO_2/C_{60} bilayer QCM electrode was eventually coated with a TiO_2 gel layer. Subsequently, Cyt. c (10 mM PBS, 1 mg/mL, pH 7.0) was adsorbed on the TiO_2/C_{60} nanohybrid layered electrode by immersing for 20 min at 25 °C. In the QCM

measurements, a decrease in frequency, which indicates the formation of one of the ultrathin layers of TiO_2 , C_{60} and Cyt. c, was observed at each of the deposition steps. In the case of the only- TiO_2 gel layer without the adsorption of fullerene, the deposition procedure was repeated three times, and then, the film was immersed in Cyt. c solution, rinsed thoroughly with deionized water and dried with nitrogen gas, as shown in Figure 1.

UV-vis measurements were performed using a Lambda 35 spectrophotometer to monitor the stepwise film assembly. Before the deposition process, a quartz plate was cleaned with concentrated sulfuric acid (96 %), thoroughly washed with pure deionized water, and subjected to sonication treatment with 1 wt. % ethanolic KOH (ethanol/water = 3:2, v/v) for 30 min. It was then washed with ethanol and pure deionized water and dried under flowing nitrogen gas.

2.3 Surface morphology and contact angle

The surface morphology of the prepared films was investigated using an atomic force microscope (AFM). AFM measurements were conducted in non-contact mode using a MicroMash NSC12/Ti-Pt/15 silicon cantilever (curvature tip radius < 40 nm, tip length 15-20 µm, Spain) on a Scanning Probe Microscope JSPM-5200 at room temperature. Contact angle

measurements were conducted using a CAM 200 optical contact angle meter (KSV Instrument, USA). The contact angles described in this study are static contact angles, which were measured with the standard sessile drop technique. A water drop was made on the tip of a syringe and placed on the film surface by moving the substrate vertically until contact between the water drop and sample was achieved. The volumes of the water droplets were maintained at 1 μ L, and the image was obtained using a CCD camera.

2.4 Cyclic voltammetry measurement

A CompactState electrochemical analyzer (Ivium Technologies, Netherlands) was used for cyclic voltammetry (CV) measurements with a typical three-electrode cell. The reference and counter electrodes consisted of a 3-M NaCl Ag/AgCl electrode and a 0.5-mm diameter platinum (Pt) wire, respectively. The QCM electrode modified with the thin film was used as the working electrode. CV measurements were collected in phosphate buffer solution (10 mM, pH 7), which was thoroughly purged with nitrogen gas before performing measurements.

3. Results and discussion

3.1 Immobilization of Cyt. c on the C_{60} hybrid TiO_2 gel layer

As shown in Figure 2, the sequential adsorption of Ti(O-ⁿBu)₄, C₆₀, and Cyt. c. result in QCM frequency changes. The change in frequency shown in Figure 2a represents the change that occurs because of the adsorption of three cycles of TiO₂ and Cyt. c. The QCM frequency decreases linearly as the adsorption cycle increases, indicating consistent growth of the TiO₂ gel multilayer film and efficient immobilization of Cyt. c on the TiO₂ gel layer. The average frequency change by $Ti(O^{-n}Bu)_4$ adsorption was 14 ± 2 Hz, and that by Cyt. c. adsorption was 144 ± 18 Hz. In the current setup, a QCM frequency decrease of 1 Hz is estimated to correspond to an increase in the thickness (the unit is Angstroms, Å) of $0.273/\rho$, where ρ is the density (g/cm³) of the adsorbed film [51]. The thickness of the TiO₂ gel layer was measured to be 0.67 ± 0.1 nm based on the frequency 42 ± 6 Hz calculated from the bulk density of the TiO₂ gel (1.7 g/cm³). Similarly, the thickness of the Cyt. c layer adsorbed on the TiO₂ gel layer is estimated to be approximately 3 nm when the density of the protein layer was assumed to be approximately 1.3 g/cm³[55]. Furthermore, the adsorption density of the Cyt. c can be calculated from the QCM frequency change ($\Delta F = 144 \text{ Hz}$) by the mass of the adsorbed Cyt. c, corrected for the molecular weight (MW: 12384) and size (2.5×2.5×3.7 nm³) of the Cyt. c as a globular shape with a diameter of ~ 3 nm and a surface area of 0.32 cm² for both sides of the QCM electrode [52]. Therefore, we postulated that the Cyt. c layer was densely absorbed on the TiO_2 gel, with 0.196 Cyt. c molecules per 1 nm². This value was estimated to correspond to 153 % of the theoretical adsorption density (0.128 Cyt. c molecules/nm²) of the Cyt. c adsorbed on the TiO_2 gel and can thus be considered to exhibit a very densely covered protein layer.

Figure 2b shows the change in the QCM frequency for the sequential adsorption of Ti(O-ⁿBu)₄, C₆₀, and Cyt. c. As expected, the QCM frequency linearly decreases during the adsorption process of the above mentioned molecules, indicating the extremely regular growth of the $TiO_2/C_{60}/TiO_2$ gel film and the successful immobilization of Cyt. c on the fullerene hybrid TiO₂ gel layer. The frequency change from the TiO₂ layer formed by the first cycle of $Ti(O^{-n}Bu)_4$ was measured to be 11 ± 3 Hz. Then, the frequency changes for C_{60} and the third cycle of $Ti(O^{-n}Bu)_4$ were 25 ± 7 Hz and 15 ± 4 Hz, respectively, and, eventually, 146 ± 25 Hz for Cyt. c. Corresponding to the frequency change by the adsorption of each molecule, the change in the thickness during the adsorption process was also investigated. The thicknesses of the TiO_2 gel layers were calculated to be 0.18 ± 0.05 and 0.24 ± 0.06 nm for the first and third cycles, respectively. The thickness of the TiO₂ gel layer generated during the third cycle was 1.36 times thicker than that of the first cycle. The discrepancy in the thickness might be induced by either desorption of the TiO2 gel during the washing and

hydrolysis step or by the enhanced surface area according to the formation of the C_{60} adsorption layer.

The thickness of the C_{60} layer was calculated to be 0.43 ± 0.12 nm based on the frequency, which was 25 ± 7 Hz, as calculated from the C_{60} layer density (1.6 g/cm³). The occupied C_{60} molecules on the TiO₂ gel layer show an adsorption density of 0.47 C₆₀ molecules per nm². This value was estimated to correspond to 59 % of the theoretical adsorption density (0.79 C₆₀ molecules/nm²) of the C₆₀ molecules adsorbed on the TiO₂ gel. This finding can be attributed to the separation between the C₆₀ molecules caused by the repulsive force during the adsorption on the TiO₂ gel layer while maintaining a sufficient distance between the C₆₀ molecules. Therefore, we can conclude that the C₆₀ molecules constitute a closely packed monolayer of spherical particles with diameters of ca. 1 nm, similar to the adsorption of Cyt. c on the TiO₂ gel. The thickness and adsorption density of the Cyt. c layer adsorbed on the TiO₂/C₆₀/TiO₂ layers were estimated to be reach to 3.1 nm and 0.199 Cyt. c molecules per nm², corresponding to 155 % of the theoretical adsorption density, which is 0.128 Cyt. c molecules per nm². Figure 2c and 2d show that the QCM frequency shifts caused by the adsorption of C₆₀ and Cyt. c on the TiO₂ gel films with different thicknesses depend on the cycles. The total QCM frequency shifts that occurred during the TiO2 gel film preparation were 11 ± 3 Hz, 40 ± 7 Hz, and 68 ± 6 Hz for 1-cycle, 3-cycle, and 5-cycle TiO_2 gel films, respectively. As the adsorption cycle increases, the thickness of the prepared films also obviously increases.

Regardless of the changes in the film thickness, the QCM frequency shifts resulting from the adsorption of C₆₀ on the TiO₂ gel films was saturated within approximately 20 min, and almost the same frequency change was observed: QCM frequency shifts of 24, 26, and 25 Hz were observed for 1-cycle, 3-cycle, and 5-cycle TiO₂ gel films, respectively, as shown in Figure 2c. These results revealed that the C₆₀ molecules only adsorbed on the surface of the TiO₂ gel films. As observed for the C₆₀ adsorption on the TiO₂ gel films, the adsorption of Cyt. c on the TiO₂ gel films was also saturated within approximately 20 min and showed very similar frequency changes for all of the TiO₂ gel films with different thicknesses (Figure 2d). As mentioned above, the QCM frequency shift is caused by the adsorption cycles, and thus, the frequency shifts for the TiO₂ gel films subjected to 1-cycle, 3-cycles, and 5-cycles were 147 Hz, 149 Hz, and 143 Hz, respectively. These results indicate that Cyt. c adsorbed on the obtained on the surface of the TiO₂ gel films only. To verify the efficient immobilization of Cyt. c on the TiO₂ gel layer, we also measured the UV-vis absorption spectra of the Cyt. cadsorbed TiO₂/C₆₀/TiO₂ nanohybrid film. The absorption peak was observed at 409 nm and

was clearly demonstrated to be the 'Soret' band, which originates from hemeprotein, which exhibits a strong absorption band [51]. In Figure 3a, the UV-vis absorption spectra display the absorption changes resulting from the adsorption of Ti(O-ⁿBu)₄ and Cyt. c. A broad absorbance band at approximately 230 nm is attributed to the formation of the TiO2 gel layer and linearly increased with the deposition cycles, indicating the preparation of regular TiO2 gel films during the consecutive deposition steps. An increase in the UV-vis absorbance intensity upon Cyt. c adsorption was clearly observed at 409 nm and is attributed to the 'Soret' band and thus originates from a heme unit. The absorption peak of the 'Soret' band has the same wavelength range as that of native Cyt. c in phosphate buffer solution (10 mM, pH 7.0). This result clearly shows that the native characteristics of Cyt. c is preserved on the TiO₂ gel layer without any conformational change or degradation. The increase in the absorbance intensity ($\Delta Abs = 0.0068$) and the molar extinction coefficient at 409 nm ($\epsilon = 106$ mM⁻¹cm⁻¹) correspond to the number of immobilized Cyt. c molecules on the TiO₂ gel layer [53]. The density of the Cyt. c adsorbed on one side of the quartz plate was found to be 0.192 Cyt. c molecules per nm², corresponding to 150 % of the theoretical adsorption density of the Cyt. c (0.128 molecules/nm²); this result is almost consistent with that determined based on the QCM frequency data (0.196 Cyt. c molecules/nm²). The UV-vis spectral changes resulting from the adsorption of Ti(O-ⁿBu)₄, C₆₀, and Cyt. c. also showed increased absorbance intensity during the consecutive deposition process, confirming the completely regular nanohybrid film assembled using TiO₂ gel, C₆₀, and Cyt. c (Figure 3b). The broad absorbance bands observed at 200~300 nm are ascribed to the TiO₂ gel layer. Additionally, after the deposition of C₆₀ on the TiO₂ gel layer, the UV-visible spectrum displayed an increase in absorption in the near UV and visible regions, although the absorption of the TiO₂ gel increased only in the near UV region. Interestingly, the UV-visible spectrum collected after the additional deposition of Ti(O-ⁿBu)₄ on the C₆₀ layer displayed an increased absorption peak from the only-TiO₂ gel layer in the near UV region, without any change in the absorbance characteristics of C₆₀, as shown in the inset in Figure 3b. Assuming that the C₆₀ molecules strongly absorb on the TiO₂ gel layer through chemical interactions, this finding can be considered to step from the interaction between the double bond of C₆₀ and the ionic species -Ti-O in the TiO₂ gel layer (Figure S3). If C₆₀ molecules are adsorbed on the TiO₂ gel layer by relatively weak interactions, such as Van der Waal's forces and/or physical adsorption, C₆₀ molecules could be readily desorbed during the deposition process of Ti(O-ⁿBu)₄ in toluene/ethanol (1/1, v/v) solution. Although the complex is formed by strong chemical interactions with the TiO₂ gel layer (the carboxylic groups can be covalently bound to the titanium atoms, -Ti-O-OC-R), we occasionally observe a decrease in the absorbance after the adsorption of $Ti(O^{-n}Bu)_4$ [53]. An increase in absorbance ($\triangle Abs = 0.0069$) resulting from Cyt. c adsorption was observed at 409 nm. The Cyt. c molecules adsorb at a density of 0.195 molecules per nm² on one side of the quartz plate, corresponding to 152 % of the theoretical adsorption density of the Cyt. c.; this finding indicates the adsorption of an excess amount of Cyt. c on the TiO2 gel layer. This excess adsorption of Cyt. c. is considered to be the result of a significant strong electrostatic interaction between the positively charged Cyt. c and the negatively charged TiO₂ gel layer. To further establish the effect of C₆₀ adsorption, we next examined the UV-vis spectrum of 10-μM C₆₀ in toluene and C₆₀ immobilized onto the TiO₂ gel layer. As shown in Figure 3d, two small bands at 261 and approximately 330 nm were observed after the deposition of C₆₀. Unfortunately, the band at approximately 330 nm is difficult to identify because it overlaps with the noise peak of the spectrophotometer. Nonetheless, these bands are very similar to those detected at 284 and 338 nm in a 10-µM toluene solution of C_{60} (Figure 3c). The blue shift suggests that the C_{60} molecules are strongly adsorbed on the TiO₂ gel layer by chemical interactions.

3.2 Surface morphology and contact angle

To increase the accuracy of the observations of the surface morphology, AFM measurements were conducted for each of the films prepared on a silicon wafer. Figure 4 and Figure S2 show the 3D and 2D AFM images of the film after the deposition of $Ti(O^{-n}Bu)_4$, C_{60} , and Cyt. c. While the surface image of the only- TiO_2 gel layer reveals extremely smooth morphology with a root-mean-square (RMS) roughness of 0.163 nm (Figure 4a), there is no significant change in the overall morphology of the films before or after C_{60} adsorption (Figure 4b). Although the presence of C_{60} molecules was not identified, the RMS roughness slightly increased to 0.212 nm after the deposition of the C_{60} molecules. We suggest that the C_{60} molecules might be adsorbed into the TiO_2 gel layer at the single particle level without aggregation.

Additionally, the surface after another deposition of $Ti(O^{-n}Bu)_4$ on the TiO_2/C_{60} layer was observed to be extremely smooth, and the RMS roughness was slightly decreased to 0.198 nm compared with the C_{60} layer (Figure 4c). Interestingly, in the final process, the RMS roughness increased to 0.438 nm after the deposition of Cyt. c, and the surface was densely covered with the adsorbed Cyt. c molecules (Figure 4d).

The contact angle facilitates better understanding of the surface properties in terms of the interactions between the prepared surfaces and liquids. The water droplets on the film after

the deposition of Ti(O-ⁿBu)₄, C₆₀, and Cyt. c on a quartz palate were formed as in Figure 5a. While the contact angle of $21 \pm 5^{\circ}$ for the TiO_2 gel layer is 5° , which agrees with the high hydrophilicity of the abundant hydroxyl group (-Ti-OH moieties) in the TiO2 gel (Figure 5a), the deposition of the C₆₀ molecules on the hydrophilic TiO₂ gel layer sharply increased the surface contact angle to 93 \pm 6° (Figure 5a and Figure S2). The C₆₀ layer exhibits very different wetting behavior than the TiO₂ gel layer. This significant change in the surface chemical features is caused by perfect modification of the TiO₂ layer by C₆₀ molecules. In contrast, the deposition of $Ti(O^{-n}Bu)_4$ on the C_{60} layer dramatically decreases the contact angle of the C_{60} layer to $24 \pm 4^{\circ}$ (Figure 5c), almost the same as that of the first TiO_2 gel layer on a quartz palate. Based on the contact angle data, we confirmed that the change in the contact angle arises from uniform and complete coverage by TiO₂ gel and C₆₀ deposition. The Cyt. c immobilized on the TiO₂ gel layer also alters the surface properties. The increase in the contact angle of the immobilized Cyt. c film $(55 \pm 3^{\circ})$ could be ascribed to an increase in the hydrophilic moieties on the protein surface and hydrophobic protein backbones.

3.3 Electrochemistry of Cyt. c

To investigate the electroactivity of the C_{60} modified electrodes, the QCM electrodes were used as working electrodes to collect CVs in PBS buffer (10 mM, pH 7) at a scan rate of 20 mV/s. Figure 6a shows the CV results for the TiO_2 -, TiO_2/C_{60} -, and $TiO_2/C_{60}/TiO_2$ -modified QCM electrodes. No obvious electrochemical response was observed for the TiO_2 gel-layered electrode in the potential range from -0.3 to 0.6 V. In contrast, the electrochemical response after the deposition of C_{60} shows a pair of current peaks that are characteristic of a weak redox system with an anodic peak potential of 0.262 V and a cathodic peak potential of 0.137 V, which are attributed to the redox system of the deposited C_{60} on the TiO_2 gel layer.

Interestingly, the electrochemical response after the deposition of Ti(O-"Bu)₄ on the C₆₀ layer has a redox peak that disappeared and induced a broadening of the capacitive current, which reveals a decrease in the electrode's effectiveness. This finding indicates that the surface is covered by TiO₂ gel, which acts as a shielding material. Figure 6b shows the CV results of (TiO₂)₃-, (TiO₂)₃/Cyt. *c*-, and (TiO₂/C₆₀/TiO₂)/Cyt. *c*-modified QCM electrodes in PBS buffer (pH 7) at a scan rate of 20 mV/s. The (TiO₂)₃ gel electrode shows no obvious electrochemical response in the potential range of – 0.3 to 0.6 V. This observation is very similar to that of the 1-cycle TiO₂ gel-layered electrode. After immobilizing Cyt. *c* on the

(TiO₂)₃ gel-layered electrode, the CVs shows a pair of redox peaks with anodic and cathodic peak potentials at 0.226 V and 0.162 V, respectively. Cyt. c immobilization results in irreversible behavior and weakly electrochemical response for the only-TiO₂ gel-layered electrode. The formal potential (E^{o}) of Cyt. c obtained from the $(TiO_{2})_{3}$ gel matrix was estimated to be 0.197 V (vs SCE). In addition, a peak-to-peak potential separation (ΔE_p) of the redox peaks was approximately 0.064 V at a scan rate of 20 mV/s. However, a pair of well-defined quasi-reversible redox peaks of Cyt. c is clearly visible for the (TiO₂/C₆₀/TiO₂)/Cyt. c-modified electrode. The anodic and cathodic peak potentials are located at 0.222 V and 0.176 V, respectively. The formal potential (E^{o}) of Cyt. c obtained from the C₆₀ hybrid gel matrix was estimated to be 0.199 V (vs SCE), and the peak-to-peak potential separation (ΔE_p) of the redox peaks was approximately 0.046 V at a scan rate of 20 mV/s. The small ΔE_p indicates a fast electron transfer reaction between the Cyt. c. and the electrode [54]. The reversibility and capacitive currents of Cyt. c. were greatly improved compared to those of the only-TiO2 gel-modified electrode. These results suggest that the introduction of C₆₀ into the TiO₂ gel matrix increased in the electrochemical characteristics of Cyt. c. Therefore, the C₆₀ nanohybrid TiO₂ gel matrix can provide a favorable environment prompting the electrochemical characteristics of Cyt. c.

4. Conclusions

A noble method for immobilizing Cyt. c on a fullerene nanohybrid TiO₂ gel film was developed using a nanoassembly approach for improved bioelectrochemical systems of Cyt. c. The immobilization of Cyt. c and film growth were characterized by QCM, UV-vis spectroscopy, AFM, contact angle, and CV. A pair of well-defined and improved quasireversible redox peaks of Cyt. c is clearly visible for the C_{60} -modified electrode. The fullerene nanohybrid TiO₂ gel matrix can provide a favorable environment prompting the electrochemical characteristics of hemeprotein. Although improvement are still required, this new approach is a simple and useful method to prepare bioelectrochemical systems. The combination of a variety of biomaterials and fullerene nanohybrid ultrathin films will provide potential pathways for not only creating novel bioelectrochemical devices but also fabricating the elements of nanostructure materials.

Acknowledgments

This work was partly supported by PNS Technologies Inc. and the KRIBB (Korea Research Institute of Bioscience & Biotechnology) Initiative Program.

References

- Tans SJ, Verschueren AM, Dekker C. Room-temperature transistor based on a single carbon. Nature 1998;393:49–52.
- 2 Han W, Fan S, Li Q, Hu Y. Synthesis of gallium nitride nanorods through a carbon nanotube-confined reaction. Science 1997;277(5330):1287–1289.
- Hewitt CA, Kaiser AB, Roth S, Craps R, Czerw R, Carroll DL. Multilayered carbon nanotube/polymer composite based thermoelectric fabrics. Nano Letters 2012;12(3):1307–1310.
- Tokuyama H, Yamago S, Nakamura E, Shiraki T, Sufiura Y. Photoinduced biochemical activity of fullerene carboxylic acid. J Am Chem Soc 1993;115(17):7918–7919.
- 5 Williams G, Seger B, Kamat PV. TiO₂–graphene nanocomposites. UV-assisted photocatalytic reduction of graphene oxide. ACS Nano 2008;2(7):1487–1491.

- 6 Dai H. Carbon nanotubes: Synthesis, integration, and properties. Acc Chem Res 2002;35(12):1035–1044.
- 7 Shen Y, Yang S, Zhou P, Sun Q, Wang P, Wan L, et al. Evolution of the band-gap and optical properties of graphene oxide with controllable reduction level. Carbon 2013;62:157–164
- 8 Menon M, Srivastava D. Williams G, Seger B, Kamat PV. Carbon nanotube "T Junctions": Nanoscale metal-semiconductor-metal contact devices. Phys Rev Lett 1997;79(22):4453–4456.
- Yamada T, Makiomoto N, Sekiguchi A, Yamamoto Y, Kobashi K, et al. Hierarchical three-dimensional Layer-by-Layer assembly of carbon nanotube for integrated nanoelectronic devices. Nano Letters 2012;12(9):4540–4545.
- 10 Collins PG, Arnold MS. Avouris P. Engineering carbon nanotubes and nanotube circuits using electrical breakdown. Science 2001;292(5517):706–709.
- Bradley K, Gabriel J-C P, Grüner G. Flexible nanotube eledtronics. Nano Letters 2003;3(10):1353–1355.
- 12 Tseng Y-C, Xuan P, Javey A, Malloy R, Wang Q, Bokor J, Dai H. Monolithic integration of carbon nanotube devices with silicon MOS techology. Nano Letters 2004;4(1):123–127.
- Petersen EJ, Tu X, Dizdaroglu M, Zheng M, Nelson BC. Protective roles of silgle-wall carbon nanotube in ultrasonication-induced DNA base damage. Small 2013;9(2):205–208.
- 14 Shi X, Sitharaman B, Pham QP, Liang F, Wu K, Edward Billups W, Wilson LJ, Mikos AG. Fabrication of porous ultra-short single-walled carbon nanotube nanocomposite scaffolds for bone tissue engineering. Biomaterials 2007;28(28):4078–4090.

- Jan E, Kotov NA. Successful differentiation of mouse neural stem cells on Layer-by-Layer assembled single-walled carbon nanotube composite. Nano Letters 2007;7(5):1123–1128.
- 216 Zhang H, Cao G, Wang Z, Yang Y, Shi Z, Gu Z. Growth of manganese oxide nanoflowers on vertically-aligned carbon nanotube arrays for high-rate electrochemical capacitive energy storage. Nano Letters 2008;8(9):2664–2668.
- 17 Chen Z, Yuan Y, Zhou H, Wang X, Gan Z, Wang F, Lu Y. 3D nanocomposite architectures from carbon-nanotube-threaded nanocrystals for high-performance electrochemical energy storage. Adv Matter 2014;26(2):339–345.
- 18 Qian ZS, Shan XY, Chai LJ, Ma JJ, Chen JR, Feng H. DNA nanosensor based on biocompatible graphene quantum dots and carbon nanotubes. Biosens Bioelectron 2014;60:64–70.
- 19 Ghoreishi SM, Attaran AM, Amin AM, Khoobi A. Multiwall carbon nanotube-modified electrode as a nanosensor for electrochemical studies and stripping voltammetric determination of an antimalarial drug. RSC Adv 2015;5:14407–14415.
- 20 Coleman JN, Khan U, Blau WJ, Gun'ko YK. Small but strong: A review of the mechanical properties of carbon nanotube–polymer composites. Carbon 2006;44(9):1624–1652.
- 21 Istracte OM, Raton KR, Khan U, O'nell A, Bell AP, Coleman JN. Reinforcement in melt-processed polymer–graphene composites at extremely low graphene loading level. Carbon 2014;78:243–249.
- 22 Chen T, Qui L, Cai Z, Gong F, Yang Z, Wang Z, Peng H. Intertwined aligned carbon nanotube fiber based dye-sensitized solar cells. Nano Letters 2012;12(5):2568–2572.

- 23 Cui K, Anisimov AS, Chiba T, Fujii S, Kataura H, Nasibulin AG, et al. Air-stable highefficiency solar cells with dry-transferred single-walled carbon nanotube films. J Mater Chem A 2014;2:11311–11318.
- 24 Cho D-Y, Eun K, Choa S-H, Kim H-K. Highly flexible and stretchable carbon nanotube network electrodes prepared by simple brush painting for cost-effective flexible organic solar cells. Carbon 2014;66:530–538.
- 25 Tong SW, Mishra N, Su CL, Nalla V, Wu W, Ji W, et al. High-performance hybrid solar cell made from CdSe/CdTe nanocrystals supported on reduced graphene oxide and PCDTBT. Adv Funct Mater 2014;24(13):1904–1910.
- 26 Kroto HW, Heath JR, Obrien SC, Curl RF, Smalley RE. C₆₀: Buckminsterfullerene. Nature 1985;318:162–163.
- 27 Goeb S, Bivaud S, Dron PI, Baladier J-Y, Chas M, Sallé M. A BPTTF-based self-assembled electron-donating triangle capable of C₆₀ binding. Chem Commun 2012;48:3106–3108.
- 28 Chen CC, Lieber CM. Synthesis of pure 13C₆₀ and determination of the isotope effect for fullerene superconductors. J Am Chem Soc 1992;114(8):3141–3142.
- 29 Haddon RC. Electronic structure, conductivity and superconductivity of alkali metal doped (C₆₀). Acc Chem Res 1992;25(3):127–133.
- 30 Johnson RD, Bethune DS, Yannoni CS. Fullerene structure and dynamics: a magnetic resonance potpourri. Acc Chem Res 1992;25(3):169–175.
- 31 Uritu CM, Varganici CD, Ursu L, Coroaba A, Nicilescu A, Dasxalu AI, et al. Hybrid fullerene conjugates as vectors for DNA cell-delivery. J Mater Chem B 2015;3:2433– 2446.
- 32 Zhao W-W, Xu J-J, Chen H-Y. Photoelectrochemical DNA Biosensors. Chem Rev 2014;114(15):7421–7441.

- 33 Andreoni A, Nardo L, Bondani M, Zhao B, Roberts JE. Time-resolved fluorescence studies of fullerene derivatives. J Phys Chem B 2013;117(24):7203–7209.
- Gao F, Zhao G-L, Yang S, Spivey JJ. Nitrogen-doped fullerene as a potential catalyst for hydrogen fuel cells. J Am Chem Soc 2013;135(9):3315–3318.
- Huang H, Wang X. Recent progress on carbon-based support materials for electrocatalysts of direct methanol fuel cells. J Mater Chem A 2014;2:6266–6291.
- 36 Sun Y, Welch GC, Leong WL, Takacs CJ, Bazan GC, Heeger AJ. Solution-processed small-molecule solar cells with 6.7% efficiency. Nat Mater 2012;11:44–48.
- Price SC, Stuart AC, Yang L, Zhou H, You W. Fluorine substituted conjugated polymer of medium band gap yields 7% efficiency in polymer–fullerene solar cells. J Am Chem Soc 2011;133(12):4625–4631.
- 38 Credginton D, Hamilton R, Atienzar P, Nelson J, Durrant JR. Non-geminate recombination as the primary determinant of open-circuit voltage in polythiophene: fullerene blend solar cells: an analysis of the influence of device processing conditions. Adv Funct Mater 2011;21(14):2744–2753.
- 39 Goyal RN, Gupta VK, Bachheti N. Fullerene-C₆₀-modified electrode as a sensitive voltammetric sensor for detection of nandrolone-An anabolic steroid used in doping. Anal Chim Acta 2007;597:82–89.
- 40 Gradzka E, Winkler K, Borowska M, Plonska-Braxezinska ME, Echegoyen L. Comparison of the electochemical properties of thin films of MWCNTs/C₆₀-Pd, SWCNTs/C₆₀-Pd and ox-CNOs/C₆₀-Pd. Electrochim Acta 2013;96:274–284.
- 41 Csiszar M. Szucs A, Tolgyesi M, Mechler A, Nagy JB, Novak M. Electrochemical reactions of cytochrome *c* on electrodes modified by fullerene films. J Electoanal Chem 2001;497:69–74.

- 42 Jain R, Rather JA, Vikas AD. Highly sensivive voltammetric sensor fullerene modified glassy carbon electrode for determination of cefifizoxime in solubilized system. Electoanalysis 2010;22(21):2600–2606.
- 43 Afreen S, Muthoosamy K, Manickam S, Hashim U. Functionalized fullerene (C₆₀) as a potential nanomediator in the fabrication of highly sensitive biosensors. Biosens Bioelectron 2015;63:354–364.
- 24 Zhong X, Yuan R, Chai Y. *In situ* spontaneous reduction sythesis of spherical Pd@Cys-C₆₀ nanopariticles and its application in nonenzymatic glucose biosensors. Chem Commun 2012;48:597–599.
- 25 Zhang H, Fan L, Yang S. Significantly accelerated direct electron-transfer kinetics of hemoglobin in a C₆₀-MWCNT nanocomposite film. Chem Eur J 2006;12:7161–7166.
- 46 Lanzellotto C, Favero G, Antonelli ML, Tortolini C, Cannistraro S, Coppari E, Mazzei F.
 Nanostructured enzymatic biosensor based on fullerene and gold nanoparticles:
 Preparation, characterization and analytical applications. Biosens Bioelectron
 2014;55:430–437.
- 47 Bijuab V. Chemical modifications and bioconjugate reactions of nanomaterials for sensing, imaging, drug delivery and therapy. Chem Soc Rev 2014;43:744–764.
- 48 Yang D-H, Park CS, Min JH, Oh MH, Yoon YS, Lee S-W, Shin JS. Fullerene nanohybrid metal oxide ultrathin films. Curr Appl Phys 2009;9:e132–135.
- 49 Yang D-H, Futagami W, Mizutani N, Lee S-W, Shin JS. Fabrication of metal oxide and fullerene layer-by-layered nanocomposite films. Kobunshi Ronbushu 2012;4:171–178.
- Yang, D-H. Takahara, N. Lee S-W, Kunitake T. Fabrication of glucose TiO₂ ultrathin films by molecular imprinting and selective detection of monosaccharides. Sens Actuators B 2008; 130: 379–385.

- Yang, D-H. Takahara, N. Mizutani N, Lee S-W, Kunitake T. Fabrication of TiO₂ and cytochrome *c* alternate ultrathin films via a gas-phase surface sol-gel process. Chem Lett 2006; 35(9): 990–991.
- 52 Ichinose I, Takaki R, Kuroiwa K, Kunitake T. Electrostatic adsorption of cytochrome *c* on ultrathin ZrO₂-gel layers and preparation of alternate multilayers. Langmuir 2003; 19: 3883–3888.
- Araki K, Yang, D-H. Wang T, Selyanchyn R, Lee S-W, Kunitake T. Self-assembly and imprinting of macrocyclic molecules in layer-by-layered TiO₂ ultrathin films. Anal Chim Acta 2013; 779: 72–81.
- Wang Y, Qian K, Guo K, Kong J, Marty J-L, Yu C, Liu B. Electrochemistry and biosensing of cytochrome *c* immobilized in macroporous materials. Microchim Acta 2011; 175: 87–95.
- Lvov Y, Ariga K, Ichinose I, Kunitake T. Molecular film assembly via layer-by-layer adsorption of oppositely charged macromolecules (linear polymer, protein and clay) and concanavalin A and glycogen. Thin Solid Films 1996; 284-285: 797–801.

Figure captions

Figure 1. Schematic illustration of the immobilization of Cyt. c onto fullerene nanohybrid ultrathin films by the surface sol-gel process.

Figure 2. QCM frequency shifts resulting from the surface modification procedure of Cyt. c (a) on a 3 cycle TiO₂ gel film ((TiO₂)₃/Cyt. c) and (b) on a fullerene nanohybrid TiO₂ gel film ((TiO₂/C₆₀/TiO₂)/Cyt. c). QCM frequency shifts resulting from the adsorption of (c) C₆₀ and (d) Cyt. c on TiO₂ gel films with different thicknesses.

Figure 3. UV-vis spectral changes caused by the deposition of (a) $Ti(O^{-n}Bu)_4$ and Cyt. c and (b) $Ti(O^{-n}Bu)_4$, C_{60} , and Cyt. c, respectively. Insets (a) and (b) show enlarged absorbance changes. (c) UV-vis spectrum for 10- μ M C_{60} in toluene, and inset (d) shows a UV-vis spectrum for C_{60} immobilized onto the TiO_2 gel layer after subtraction of the absorption spectrum of the TiO_2 gel layer.

Figure 4. 3D AFM images (1 μ m×1 μ m) of the 1-cycle (a) TiO₂, (b) TiO₂/C₆₀, (c) TiO₂/C₆₀/TiO₂, and (d) (TiO₂/C₆₀/TiO₂)/Cyt. c layers deposited on a plasma-treated silicon substrate.

Figure 5. Micrograph of the surface contact angle of the 1-cycle (a) TiO_2 , (b) TiO_2/C_{60} , (c) $TiO_2/C_{60}/TiO_2$, and (d) $(TiO_2/C_{60}/TiO_2)/Cyt$. c layers deposited on a quartz palate.

Figure 6. Cyclic voltammograms (tenth redox cycle) of (a) 1-cycle TiO_2 , $\text{TiO}_2/\text{C}_{60}$, and $\text{TiO}_2/\text{C}_{60}/\text{TiO}_2$ films and (b) 1-cycle TiO_2 , $(\text{TiO}_2)_3/\text{Cyt.}$ c, and $(\text{TiO}_2/\text{C}_{60}/\text{TiO}_2)/\text{Cyt.}$ c films in phosphate buffer (10 mM, pH 7) using a scan rate of 20 mV/s.

Figure 1.

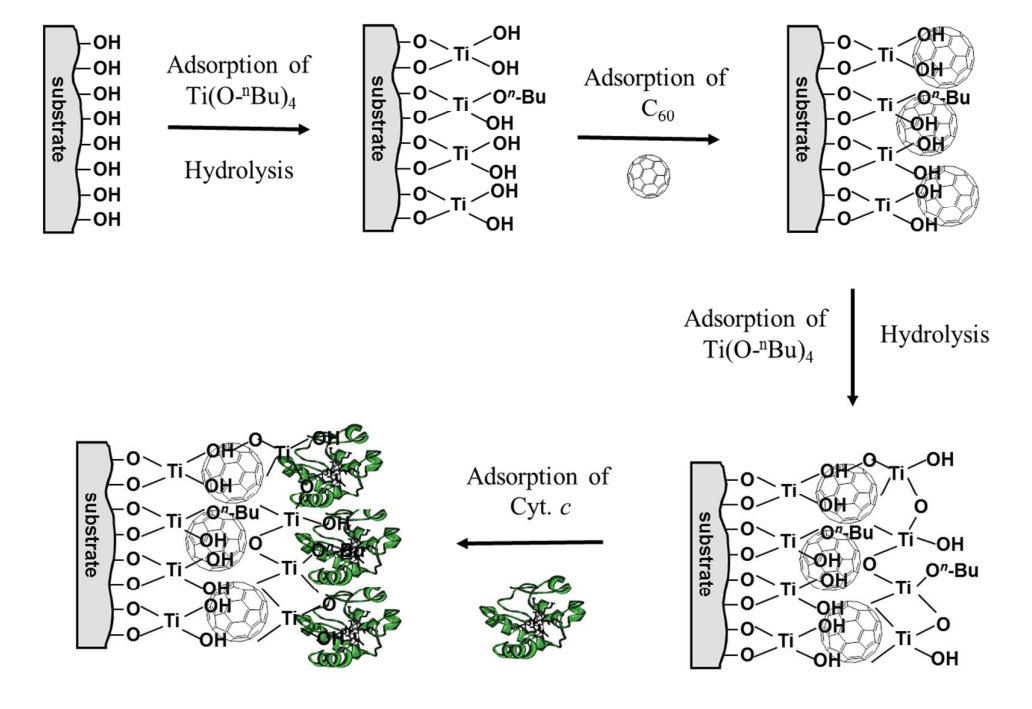


Figure 2.

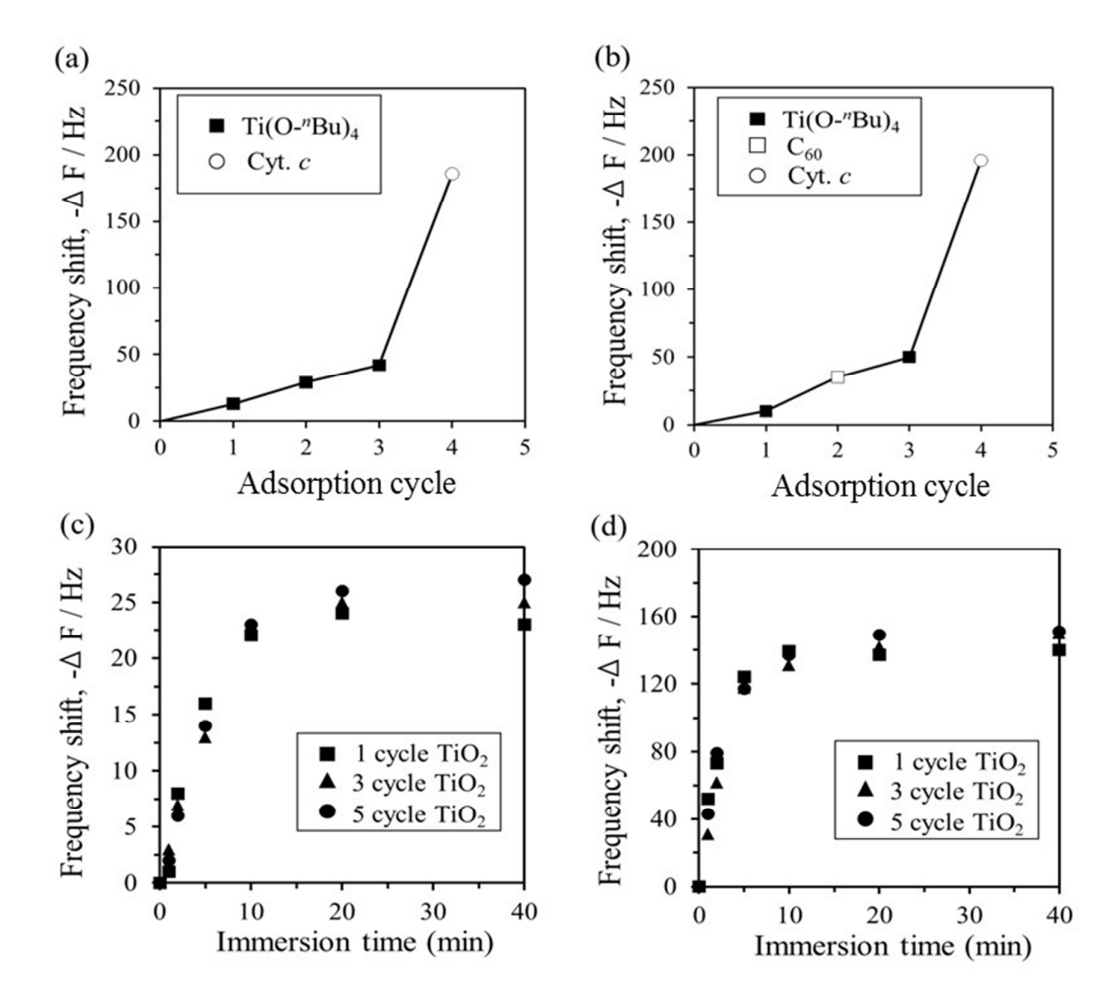
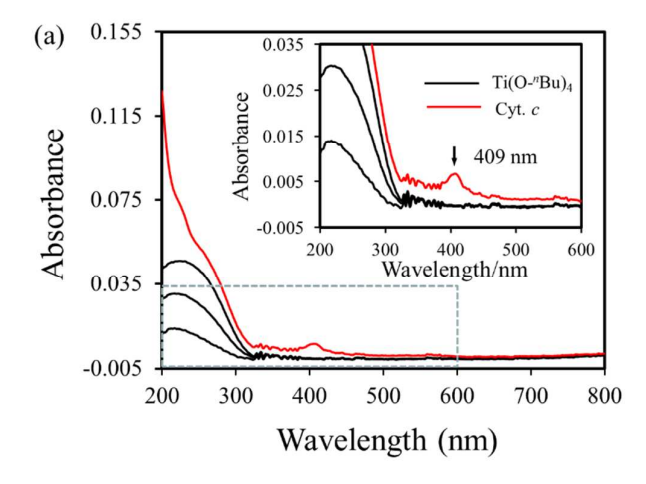
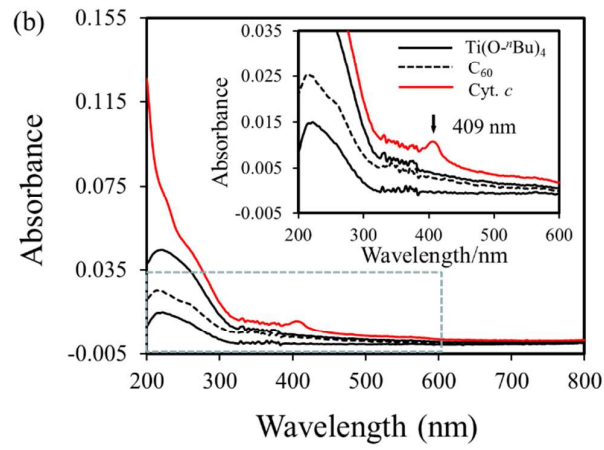


Figure 3.





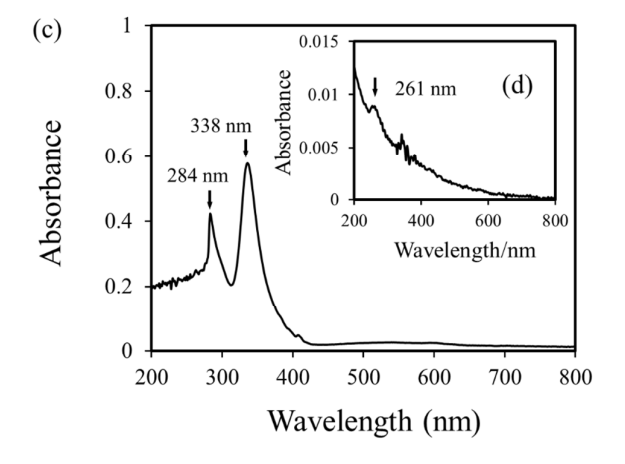


Figure 4.

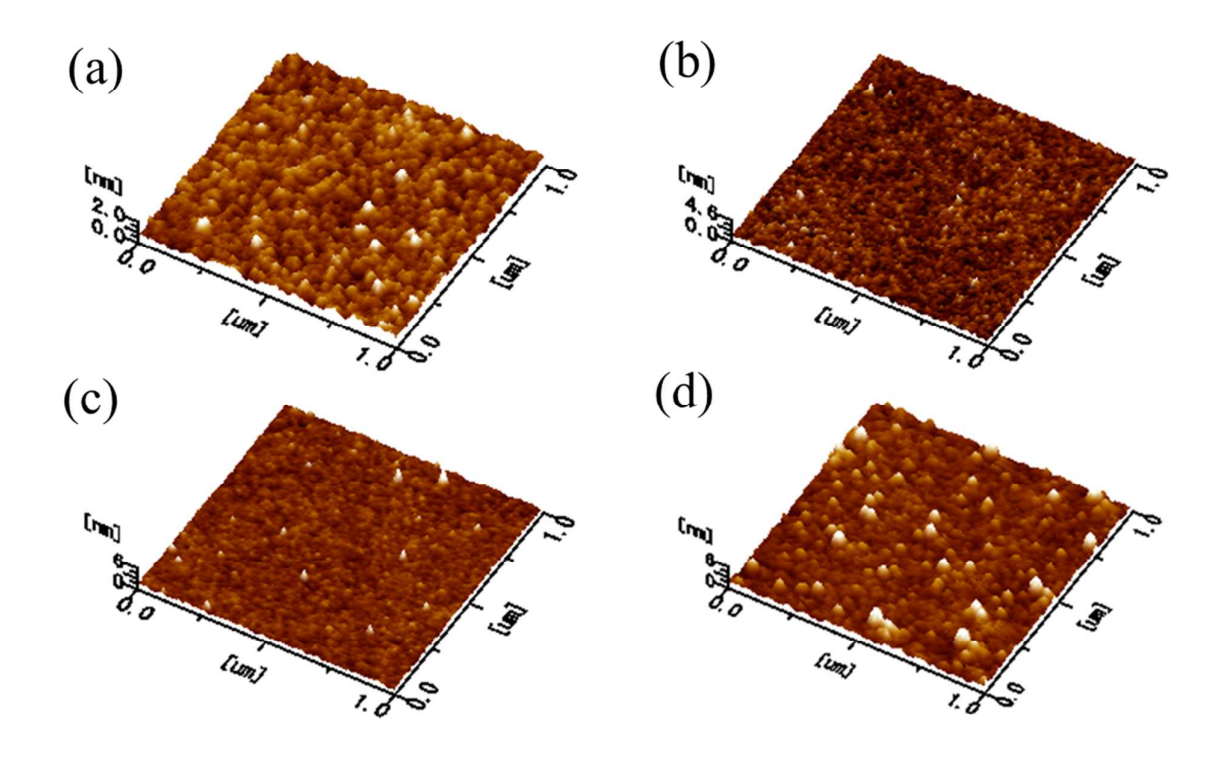


Figure 5.

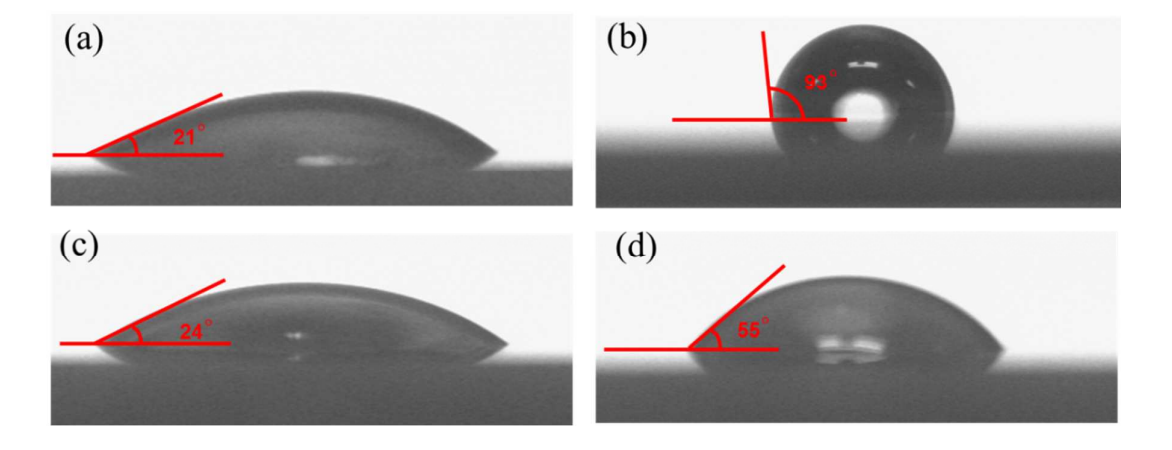
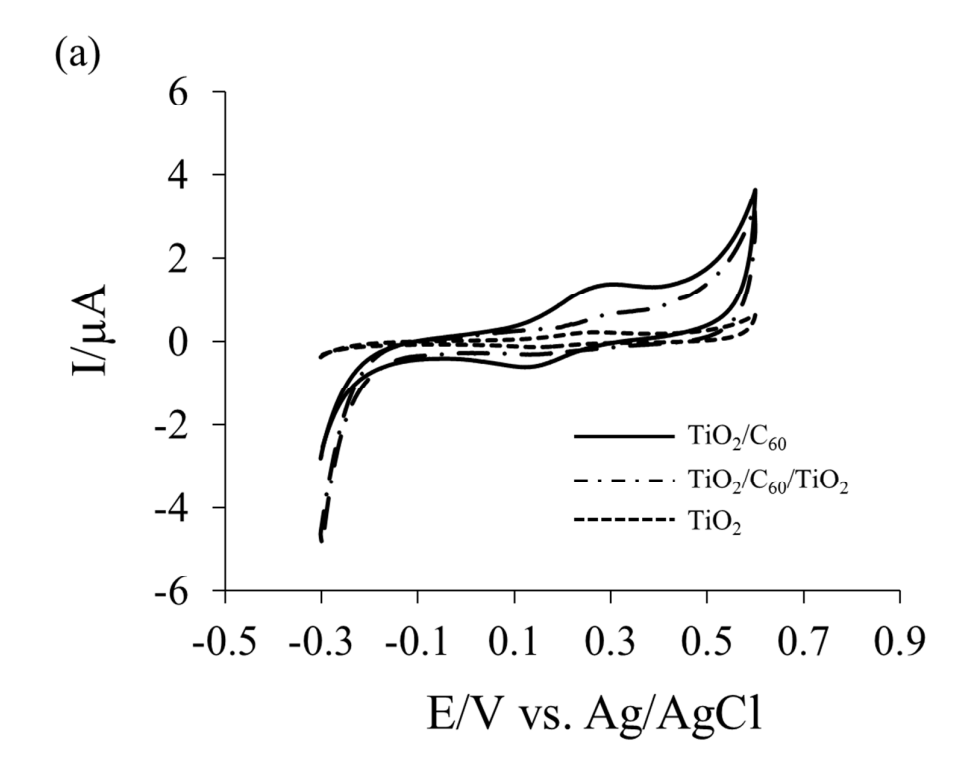
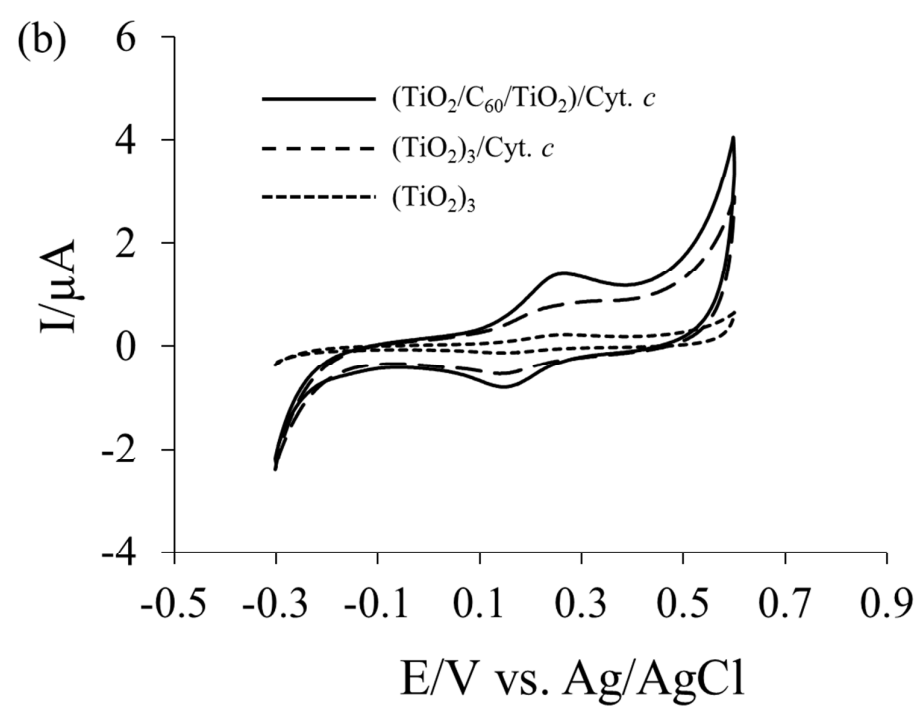


Figure 6.





Graphical Abstract

